# Hybrid copper-polyelectrolyte nanoaggregates obtained with smart block copolymers based on 4-[(hydroxyimino)aldehyde]butyl methacrylate (HIABMA) in water and acetonitrile

Polymer 306 (2024) 127197

Contents lists available at ScienceDirect

Polymer

journal homepage: www.elsevier.com/locate/polymer

# Hybrid copper-polyelectrolyte nanoaggregates obtained with smart block copolymers based on 4-[(hydroxyimino)aldehyde]butyl methacrylate (HIABMA) in water and acetonitrile

Irene Antignano [a], Stefano Casciardi [b], Francesca D'Acunzo [c,*], Alessandra Del Giudice [a], Laura Gatti [a], Patrizia Gentili [a,c], Francesco Mura [d], Agnese Ricci [a], Giancarlo Masci [a,**]

[a] Department of Chemistry, Sapienza University of Rome, P.le A. Moro 5, 00185, Roma, Italy
[b] National Institute for Insurance Against Accidents at Work (INAIL Research), Department of Occupational and Environmental Medicine, Epidemiology and Hygiene, Rome, Italy
[c] Institute of Biological Systems (ISB), Italian National Research Council (CNR), Sezione Meccanismi di Reazione, c/o Department of Chemistry, Sapienza University of Rome, Piazzale Aldo Moro 5, 00185, Roma, Italy
[d] Department of Basic and Applied Sciences for Engineering (SBAI), Sapienza University of Rome, Via Antonio Scarpa 14, 00161, Rome, Italy

ARTICLE INFO

*Keywords:*
Polymeric micelles
Polyion
Polyelectrolyte
Block copolymers
Hybrid complex
Cu(II) ions
2-(Hydroxyimino)aldehyde

ABSTRACT

The AB multi-stimuli-responsive block copolymer pTEGMA-*b*-pHIABMA (TEGMA: tetra(ethyleneglycol) methyl ether methacrylate; HIABMA: 4-[(hydroxyimino)aldehyde]butyl methacrylate) comprises a hydrophilic and thermoresponsive PTEGMA block linked to the hydrophobic PHIABMA chain. The latter is endowed with slightly acidic oxime groups that potentially form complexes with metal ions. Here we investigate the formation of hybrid Cu(II)-polymer nanoaggregates both in water and in acetonitrile. Cu(II) ions are quantitatively and rapidly incorporated, in the presence of a base, into pre-formed polymeric *core-shell* micelles (30 nm diameter by DLS) in water up to 1:2 metal-to-ligand stoichiometry. The pKa of the polymer is decreased from ≅11.2 to 4.65 due to interaction with Cu(II) and the complex is shown to involve oximate ions. The thermoresponsivity of the polymeric micelles remains unchanged with Cu(II) complexation and allows an easy separation by flocculation of the hybrid complex. Moreover, nanoaggregates (D = 20 nm) form in acetonitrile from the fully solubilized copolymer interacting with $Cu(OAc)_2$. The 1:2 Cu(II)/ligand stoichiometry is confirmed with the Job graphical method. Characterization of the hybrid micelles was carried out by UV–Vis spectrometry, DLS, TEM, STEM and SAXS. Quantitative release of Cu(II) in acidic conditions is demonstrated both in water and in acetonitrile. Full recovery of the free metal ions and of intact polymeric micelles is achieved through centrifugal filtration of the aqueous preparation, as a *proof-of-concept* for a recyclable system for metal uptake and release. Furthermore, $Cu^0$ nanoparticles of 5–10 nm are obtained through reduction of Cu(II) within the micelles with ascorbic acid in aqueous solution.

## 1. Introduction

Self-assembly of stimuli-responsive block copolymers into well-defined nanostructures with different morphologies and properties is extensively studied and regarded as a versatile tool in a wide range of technologies [1–6]. In the last decades, the self-assembling properties of metal-interacting polymers have been widely studied in order to use such materials in the biomedical field as nanocarriers or in catalysis as nanoreactors [7–11]. They are also used in the environmental sector, to eliminate heavy metals from wastewater [12–14], and for the generation of metal nanoparticles [15–19]. Furthermore, transition metal ion coordination can be viewed as a tool for directing the assembly of synthetic nanomaterials [20]. In this context, Cu(II) is particularly relevant due to its environmental impact and in view of its effects on human health [8,21–23].

Metal-ligand coordination can occur with preformed nanoaggregates [21,24], or it can constitute in itself the chemical stimulus that triggers self-assembly of the polymeric chains [6,8,14]. As an example,

* Corresponding author.
** Corresponding author.
*E-mail addresses:* francesca.dacunzo@cnr.it (F. D'Acunzo), giancarlo.masci@uniroma1.it (G. Masci).

https://doi.org/10.1016/j.polymer.2024.127197
Received 14 March 2024; Received in revised form 21 May 2024; Accepted 21 May 2024
Available online 23 May 2024

metal-mediated self-assembly of chelating double-hydrophilic block copolymers (DHBCs) has attracted increasing attention [10]. DHCBs are made of a neutral hydrophilic block like poly(ethylene oxide) (PEO), Poly(N-isopropylacrylamide) (PNIPAAM), poly[oligo (ethylene glycol) methyl ether methacrylate] (POEGMA), poly(2-iso-propyl-2-oxazoline) (PiPOX) and a block able to interact with metal ions. Regarding this latter, the most used polymers are based on carboxylic or other functional groups that can be negatively ionized, such as poly(acrylic acid) (PAA) or poly(2-acrylamidoglycolic acid) (PAGA), and based on amine functional groups that easily interact with the metal ions through their free electron doublet on the nitrogen atom, like poly(2-vinylpyridine) (P2VP), poly(ethylene imine) (PEI), or poly(2-(dimethylamino)ethyl methacrylate) (PDMAEMA) [10]. Moreover, since the polyelectrolytic ligands are pH-responsive, they may have different affinities towards different metals depending on the pH of the environment. Usually, when the pH of the solution decreases, metal retention decreases. This is due to the competition of $H^+$ with the metal.

Loading the nanoaggregates with metal ions yields hybrid homogeneous organic-inorganic materials in a simple way. Furthermore, tailor-made nanostructures with different sizes and morphologies can be obtained by varying the metal/ligand ratio, the length of the ligand block, the type of metal cation and the block copolymer concentration [11].

Oximes have been shown to be good metal ligands and the chemistry of oxime/oximate metal complexes has been widely studied, including vic-dioximes, substituted oximes, 2-pyridyl oximes, and cyanoximes [25–30].

Furthermore, polymeric materials bearing oxime-based ligand moieties are widely used to interact with metal ions serving diverse purposes. Amidoxime-modified polymers [13,31,32] are employed for heavy metal removal from industrial wastewater, whereas poly (salicylaldehyde-acrylate-divinylbenzen)oxime [33] and α-hydroxy oxime-containing cellulose [34] are employed in extraction chromatography of metal ions from aqueous solutions. However, to the best to our knowledge, there is no report of oxime-containing block copolymers nanoaggregates loaded with Cu(II) (or with other metal ions).

In our recent work several amphiphilic block copolymers encompassing the 4-[(hydroxyimino)aldehyde]butyl methacrylate (HIABMA) repeat unit were easily and successfully synthesized via RAFT polymerization, with systematic variations in their compositions [35]. (Fig. 1, first polymer on the left as an example).

The HIABMA monomer is sensitive to pH [36], it exhibits a wavelength-dependent photochemical behavior (i.e., *E/Z* oxime isomerism and chemoselective Norrish−Yang cyclization) [36–38] and has potential for metal chelation [38]. These features make PHIABMA an interesting building block to obtain useful multi-stimuli responsive copolymers.

By exploiting the pH sensitivity of the HIA units we obtained monodisperse, stable and reversible core-shell micelles (Fig. 1). They consist of a PHIABMA hydrophobic core and a POEGMA hydrophilic shell that makes them also thermoresponsive [35].

In the present work we report our first investigation on metal ligation by polymers obtained from the HIABMA monomer (Fig. 1). We focus on Cu(II) not only in view of its relevance in diverse applications, but also because of the distinctive UV–Vis bands of its complexes, which make it

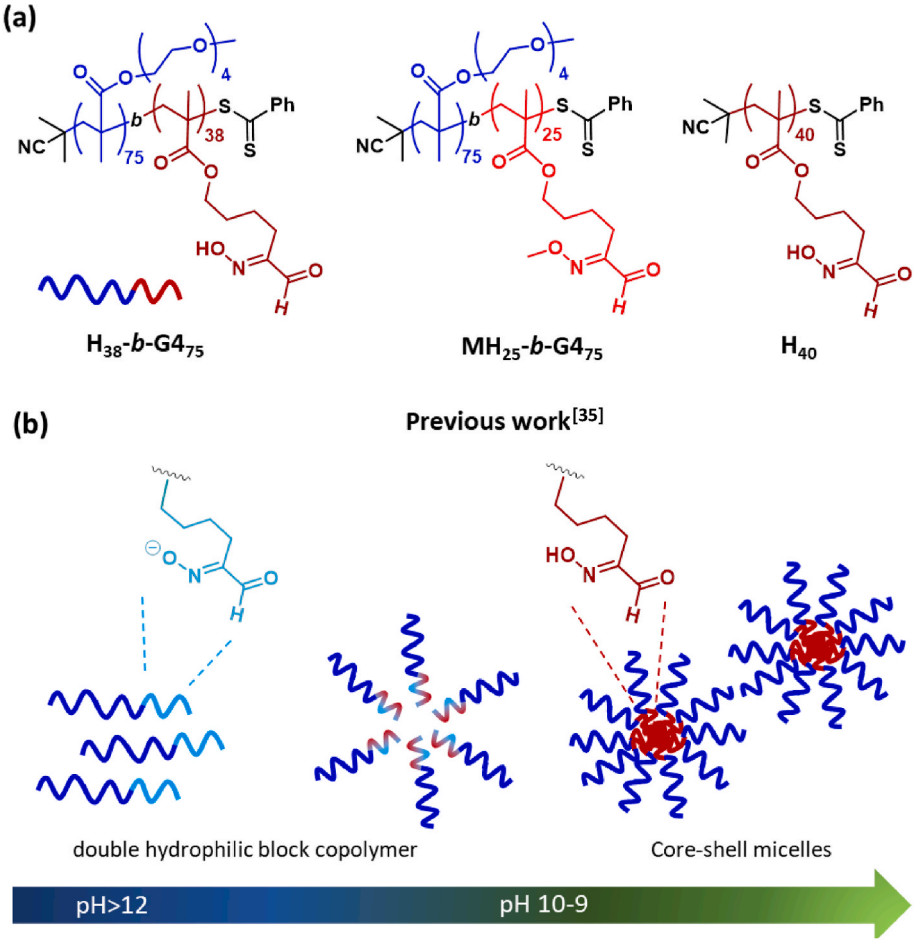


**Fig. 1.** (a) Molecular structure of the polymers in this study. **G4** = TEGMA ($OEGMA_{300}$); **H** = HIABMA (4-[(hydroxyimino)aldehyde]butyl methacrylate); **MH** = 4-[(methoxyimino)aldehyde]butyl methacrylate; The suffix next to the repeat unit abbreviation indicates the DP for each block (See SI for characterization). (b) Schematic cartoon of pH-induced micellization (PIM) method shown in our previous work [35].

a convenient choice for a first study with a new ligand. A specific block copolymer composition (**$H_{38}$-*b*-$G4_{75}$**: Fig. 1) is chosen, out of the several copolymers that we recently described [35], because it provides well defined core-shell micelles of 30 nm with the most favourable pH- and temperature responsivity. A second block copolymer (**$MH_{25}$-*b*-$G4_{75}$**; Fig. 1) is included in this study, in which an oxime ether moiety replaces free oximes, in order to investigate the relevance of the latter in the formation of metal complexes. Finally, HIABMA homopolymer **$H_{40}$** (Fig. 1) is investigated as polymeric ligand in acetonitrile.

## 2. Materials and methods

**Gel Permeation Chromatography.** GPC analyses were performed on a Hewlett Packard Series 1050 HPLC system equipped with a 1047A RI detector and a TSK gel alpha-4000 GPC column (Tosoh, Japan), using DMF with 0.1 % (w/w) LiBr as the mobile phase at a flow rate of 0.8 mL $min^{-1}$. The system was coupled to Clarity software version 6.2 (DataApex, Prague, The Czech Republic) for signal processing. Molecular weights are relative to monodisperse polyethylene oxide (PEO) standards (Agilent). The concentration of the polymeric solutions was ≈1−2 mg $mL^{-1}$. Samples were filtered through poly(vinylidene difluoride) (PVDF) syringe filters 0.45 μm, 13 mm (Lab Service, Italy) prior to analysis.

**NMR Spectrometry.** All $^1$H NMR and $^{13}$C NMR spectra were recorded in $CDCl_3$ and/or DMSO-$d_6$ on a Bruker Avance 300 spectrometer (300 MHz) or Bruker Avance NEO 400 Nanobay (400 MHz). Chemical shifts are referred to the solvent signal and expressed in parts per million (δ scale).

**Dynamic Light Scattering.** DLS data were obtained with a Brookhaven Instruments Corp. BI-200SM goniometer equipped with a BI-9000AT digital correlator using a solid-state laser (125 mW, $\lambda = 532$ nm). Measurements of scattered light were made at a scattering angle $\theta$ of 90°. The nanoaggregates formation was monitored at 25 ± 0.1 °C. The experimental duration was in the range of 5–20 min, and each experiment was repeated two or more times. Cumulant analysis or CONTIN was used to fit the data.

**UV–Vis Spectrophotometry.** Spectra were recorded on a JASCO V-530 UV–vis spectrophotometer equipped with a Peltier Jasco EHC-477T.

**TEM measurements.** All transmission electron microscopy analyses were carried out with a Tecnai 12 G2 Twin (ThermoFisher Scientific Inc), equipped with a lanthanum hexaboride thermionic electron source, operating at a primary beam maximum energy of 120 keV. Electron images and diffraction patterns were acquired with a 12 megapixels digital CMOS sensor Phurona camera (Emsis GmbH), installed in the projection chamber at the end of the magnetic lens column, which could be inserted on demand along the microscope optical axis above the viewing screen. Diffraction patterns were obtained by means of Nanoarea Electron Diffraction (NED), and the sample volume was directly selected using a highly collimated and coherent primary electron beam, controlled by condenser apertures and lenses. In this way, a very high spatial resolution could be achieved, with an electron beam diameter of a few tens of nanometers (about 30 nm). X-ray Energy Dispersive Spectrometry (XEDS) measurements were performed on a Thermo-Ultradry (ThermoFisher Scientific Inc), selecting the sample volume of interest by the same nanoarea electron beam method used in NED. All samples were prepared placing a suspension drop (10 μL) on a TEM 400 mesh Cu grid covered with a thin amorphous carbon film. Sometimes, to better visualize the polymeric particles, the negative staining was applied using phosphotungstic acid (PTA) aqueous solution 2 % w/v buffered at pH 7.3 with NaOH.

**STEM measurements.** STEM images were obtained using a ZEISS Auriga scanning electron microscope equipped with the STEM module for operation in transmission mode. The samples were deposited by drop casting on 400 mesh copper grid covered with a 20 nm amorphous carbon film (Agar Scientific) and loaded inside the electron microscope by the specific sample-holder. To get a good compromise between transmitted image resolution and a low radiation damage, the electron beam was accelerated at 20 kV, while the working distance is set around 2 mm.

**SAXS measurements.** SAXS measurements were performed at SAXSLab Sapienza with a Xeuss 2.0 Q-Xoom system (Xenocs SA, Grenoble, France), equipped with a micro-focus Genix 3D X-ray source ($\lambda = 0.1542$ nm) and a two-dimensional Pilatus3 R 300K detector (Dectris Ltd., Baden, Switzerland). The beam size was collimated to 0.5 mm × 0.5 mm and the range of scattering vector module (q), where $q = (4\pi \sin\theta)/\lambda$, 2θ being the scattering angle, was performed using silver behenate. Measurements at there sample-detector distances were performed so that the overall explored q region was $0.04\ nm^{-1} < q < 12\ nm^{-1}$. Samples were loaded into vacuum-tight quartz capillary cells with thickness 1.5 mm and measured in the instrument sample chamber at reduced pressure (~0.2 mbar) in a thermalized holder, set at 25 °C unless otherwise specified. The two-dimensional scattering patterns were subtracted for the "dark" counts, and then masked, azimuthally averaged, and normalized for transmitted beam intensity, exposure time and subtended solid angle per pixel, by using the FoxTrot software developed at SOLEIL. The one-dimensional intensity vs. q profiles were then subtracted for the solvent and cell contributions and put in absolute scale units ($cm^{-1}$) by dividing for the known thickness. The different angular ranges were merged using the SAXS utilities tool [39]. Guinier fit analysis and the indirect Fourier transform to calculate the pair distance distribution functions were performed with the SAS Data Analysis tools of the ATSAS package [40]. Attempts to describe the sample scattering according to analytical models were performed with the software packages SasView (SasView version 5.0.2) and Sasfit [41].

### 2.1. Synthesis of monomers

**4-[(hydroxyimino)aldehyde] butyl methacrylate (HIABMA)** was synthesized as previously described and purified by silica gel column chromatography. A second chromatographic purification shortly prior to polymerization is necessary to obtain high monomer conversions in RAFT polymer synthesis [35]. HIABMA was isolated as a clear viscous, colorless liquid with a 49 % yield.

$^1$H NMR (300 MHz, DMSO-$d_6$, δ): 12.92 (s, 1H, O*H*); 9.40 (s, 1H, C*H*O); 5.99 (m, 1H, C═C$H_2$), 5.65–5.66 (m, 1H, C═C$H_2$); 4.05–4.09 (t, 2H, C$H_2$O(C═O); 2.35–2.40 (t, 2H, C$H_2$–C(NOH)); 1.86 (m, 3H, C$H_3$C═$CH_2$); 1.41–1.65 (m, 4H, 2 x C$H_2$).

$^{13}$C NMR (75 mHz, DMSO-$d_6$, δ): 192.25 (*C*HO), 167.16 (*C*(O)OR), 159.71 (*C*(NOH)), 136.31 (*C*═$CH_2$), 125.81 (C═*C*$H_2$), 64.13 (*C*$H_2$O (C═O), 28.45, 21.91, 20.99, 18.34 (*C*$H_3$C═$CH_2$).

**4-[(methoxyimino)aldehyde] butyl methacrylate (MIABMA)** was obtained from HIABMA (0.20 g, 0.94 mmol). The substrate was dissolved in acetone (3.8 mL), then 0.52 g (3.8 mmol) of potassium carbonate ($K_2CO_3$) was added. The solution was left under stirring for 5 min, then 0.18 mL (1.9 mmol) of dimethyl sulfate ($Me_2SO_4$) was added dropwise. After 3 h stirring at room temperature, the reaction was stopped by adding 16 mL of water. The completeness of the reaction was confirmed by both gas chromatography (GC) and thin layer chromatography (TLC) analysis. After 30 min, further 35 mL of water was added, and the aqueous phase was extracted with 4x30 mL of diethyl ether ($Et_2O$). The combined organic phases were washed with 2x60 mL of sodium bicarbonate ($NaHCO_3$) and then with 1x60 mL of brine. Finally, the organic phase was dried over $Na_2SO_4$, filtered, and solvents removed under reduced pressure. The residue was then purified by chromatographic column on silica gel, eluted with a mixture of petroleum ether/ethyl ether (from 20:1 to 15:1 vol/vol). MIABMA (**MH**) was a viscous, colorless liquid (126 mg, 0.56 mmol, Yield = 60 %). Both *E* and *Z* configurations of oxime ether are present ($^1$H and $^{13}$C NMR).

$^1$H NMR (400 MHz, $CDCl_3$, δ): 10.12, 9.43 (s, 1H, C*H*O); 6.12 (m, 1H, C═C$H_2$); 5.57 (m, 1H, C═C$H_2$); 4.21–4.14 (2H, C$H_2$O(C═O)); 4.12, 3.83 (3H, OC$H_3$); 2.49 (t, 2H, C$H_2$C(NOH)); 1.95 (m, 3H, C$H_3$C═$CH_2$);

1.71–1.65 (m, 4H, $CH_2$).

$^{13}$C NMR (100 mHz, $CDCl_3$, δ): 190.74, 182.11 (*C*HO); 167.56 (*C*(O)OR); 159.73 (*C*(NOCH3)); 136.55 (*C*=$CH_2$); 125.43 (C=*C*$H_2$); 66.95–61.75 (NO*C*$H_3$ and *C*$H_2$O(C=O); 28.63–21.95, 18.43 (*C*$H_3$C=$CH_2$).

### 2.2. Synthesis of polymers

All polymers were obtained, as previously described, by RAFT polymerization with the Chain Transfer Agent cyanopropan-2-yl dithiobenzoate (CPDB; STREM Chemicals, Inc., BISCHHEIM, France) and with AIBN as the initiator [35]. The polymerization reactions were conducted in DMSO (previously dried on molecular sieves) under argon atmosphere in flame-sealed glass ampules at 75 °C for 7–9 h. Final volume was adjusted to 0.55–0.80 M monomer concentration. DMSO was removed by dialysis against ethyl acetate (RC tubing Spectrapor 7; MWCO = 1 kDa) and the solvent was removed in several days under high vacuum, yielding a pink oil.

**p(HIABMA) (H40).** HIABMA (75 mg, 0.35 mmol), CPDB (1.9 mg, 8.8 μmol), AIBN (0.36 mg, 2.2 μmol) and DMSO (0,640 mL).

**p(HIABMA)-*b*-pTEGMA ($H_{38}$-*b*-$G4_{75}$) and p(MIABMA)-*b*-pTEGMA ($MH_{25}$-*b*-$G4_{75}$).** The polyTEGMA (poly[tetra(ethyleneglycol)] methyl ether methacrylate: **$G4_{75}$**) block was synthesized first. [G4]/[CPDB]/[AIBN] = 75:1:0.25. After 9h at 75 °C monomer conversion was quantitative ($^1$H NMR). The resulting macro-CTA was submitted to one-pot chain elongation by simply adding HIABMA or MIABMA [HIABMA]/[G4]/[AIBN] = 40:1:0.25 and [MIABMA]/[G4]/[AIBN] = 25:1:0.25, respectively, and conducting the polymerization in the same reaction conditions. Monomer conversions were quantitative as determined by $^1$H NMR, so the composition of the copolymers was 75 TEGMA and 38 HIABMA units (**$H_{38}$-*b*-$G4_{75}$**) or 25 MIABMA units (**$MH_{25}$-*b*-$G4_{75}$**). Đ ($M_W/M_n$) = 1.19 and 1.33, respectively (GPC).

**pH-induced micellization.** Core-shell micelles were obtained from **$H_{38}$-*b*-$G4_{75}$** as previously described [35]. Briefly, 1.7 mg of polymer (Mn = 30.6 kDa; HIABMA = $6 \times 10^{-5}$ mol) was dissolved in 1 mL NaOH 0.1 M. After stirring for 30 min, the solution became clear and pH was 11. The pH was then gradually lowered by the addition of 0.1 M HCl, and the formation of nanoaggregates was monitored by DLS. The final volume was adjusted to obtain [HIABMA] = $1.8 \times 10^{-3}$ M.

**Cu(II) loading of pre-formed micelles.** Appropriate aliquots of Cu$(NO_3)_2$ or $Cu(OAc)_2$ 0.05 M in milliQ water were added under stirring to the core-shell micelles obtained by pH-induced micellization.

**Nanoaggregation with Cu(II) in acetonitrile.** The polymers **$H_{38}$-*b*-$G4_{75}$** (2.0 mg, HIABMA = $2.5 \times 10^{-6}$ mol), **$H_{40}$** (0.67 mg, HIABMA = $3.1 \times 10^{-6}$ mol) and **$MH_{25}$-*b*-$G4_{75}$** (2.8 mg, MIABMA = $2.5 \times 10^{-6}$ mol) were solubilized, respectively, in 2.5 mL, 3.1 mL and 2.5 mL of acetonitrile in a quarz cuvette (optical path 1 cm) equipped with a magnetic bar, to obtain 1 mM HIABMA or MIABMA. After about 30 min stirring, appropriate aliquots of a 10 mg $mL^{-1}$ $Cu(OAc)_2$ solution were added to explore different metal-to ligand molar ratios ([$Cu^{2+}$]/[HIA] = 0.05 to 2), recording a spectrum after each addition.

## 3. Results and discussion

### 3.1. Loading preformed micelles with Cu(II) ions

Cu(II) complexation by preformed micelles in water was initially studied. The nanoaggregates were obtained by the pH-induced micellization (PIM) of **$H_{38}$-*b*-$G4_{75}$** copolymer, as we previously described [35]. Briefly, we estimated pKa 11.2–11.3 for the copolymer (Fig. 4 in Reference 35). Therefore, at pH > 11 **$H_{38}$-*b*-$G4_{75}$** is a polyionic double-hydrophilic polymer solubilized as unimers. Micelles are then obtained by gradually lowering the pH. These micelles exhibit a well-defined *core-shell* structure with an overall diameter of 30 nm, measured by DLS. Several aliquots of a 50 mM $Cu(NO_3)_2$ or $Cu(OAc)_2$ aqueous solution were simply added to the micelle solution ([HIA] = 1.8 mM) and UV–Vis spectra were recorded 5 min after each addition. Visually, the solution remained clear and turned green from colorless. Accordingly, two bands of increasing intensity appeared at 400 and 610 nm (Fig. 2).

These absorption bands are attributed to the complexation of Cu(II) by HIA groups [42]. The band at about 610 nm is associated with the *d-d* electronic transition of complexed Cu(II) [43], that at 400 nm with the ligand-to-metal charge transfer transition (LMCT) [44]. A hint at a plausible complex geometry can be inferred from the spectral properties of the complex. The extinction coefficient at λ = 610 nm estimated from the slope of the linear trend of abs as a function of the [Cu(II)] is $\varepsilon_{610}$ = 136 $M^{-1}$ $cm^{-1}$ for the acetate and 124 $M^{-1}$ $cm^{-1}$ for the nitrate. The value of ε of the *d-d* transition bands strongly depends on the geometry of the complex. Absorption bands in octahedral complexes are generally weak (**ε** in the range 1–500 $M^{-1}cm^{-1}$) because *d-d* transitions of the type $t_{2g}$→$e_g$ are orbitally forbidden, whereas some of the *d-d* transitions in tetrahedral complexes are fully allowed and can lead to quite strong absorption, up to 5000 $M^{-1}cm^{-1}$ [45]. Therefore, the value of ε obtained for the 610 nm band is within the characteristic range of octahedral complexes. However, this geometry can undergo distortions leading to a square planar or square bipyramidal geometry. In fact, the *d-d* transitions between 600 and 700 nm are mainly attributed to a square planar geometry [46–48]. The elucidation of the Cu(II)-HIA complex structure will require a dedicated study, also involving non-polymeric HIAs.

The nature of the copper counterion strongly affects the intensity of the absorption bands as a function of R = [$Cu^{2+}$]/[HIA] (Fig. 2). In fact, at R = 0.5, $A_{max}$ (400 nm) = 1.2 with acetate, whereas a lower value of $A_{max}$ (400 nm) = 0.4 is reached at R < 0.5 with nitrate. Interestingly, the latter value increases to about 1.2 upon adding NaOAc to the nitrate solution (See Fig. S1). In other words, the acetate counterion acts as a base that favors the formation of the complex through oxime dissociation. We thereby explored the effect of pH on the spectra of a R = 0.5 mixture prepared with $Cu(NO_3)_2$. The as-prepared solution was slightly acidic (pH = 4), as expected upon addition of Lewis acid Cu(II). We adjusted the pH to 2.5 and then we added aliquots of NaOH 0.1 M, recording the UV–Vis spectra as a function of pH up to pH 8 (Fig. 3a). Then the pH was lowered again to pH 2.5 (Fig. 3b) to check for any differences between spectra recorded in the two runs (i.e. pH up and down).

Spectra in Fig. 3 exhibit the same bands as in Fig. 2. Fig. 3c shows the intensity of the 400 nm band as a function of pH. $A_{400}$ is close to zero at acidic pH and increases with increasing pH with a sigmoidal curve shape. The curves obtained by increasing/decreasing the pH in the 2.5–8.5 interval are only slightly shifted and exhibit very similar shapes, pointing at a substantially reversible process. Identical results were obtained by repeating the alkalinization experiment with $Cu(OAc)_2$ in place of $Cu(NO_3)_2$ (Fig. S2), the only difference being the pH of the as-prepared mixture (pH = 4.8, $A_{400}$ = 1.2). We thereby infer that the band at 400 nm is amenable to Cu(II)-oximate anion interactions, and that its intensity is a function of pH and is independent of the counterion in the Cu(II) salt. The curves in Fig. 3c should, then, be viewed as spectrophotometric titrations of the Cu(II)-oxime system, so that the $pK_a$ of the HIA groups in the presence of Cu(II) ions can be estimated from the vertical inflection point of the sigmoid. A non-linear fit of the experimental points in the alkalinization experiments of both Cu(II) nitrate and acetate (Fig. S3) results in an estimated pKa of 4.65. This value is more than 6 pKa units lower than that of **$H_{38}$-*b*-$G4_{75}$** (estimated pKa 11.2–11.3)[35] and is consistent with the acidity enhancement effect of up to seven orders of magnitude observed with Cu(II) on a series of 2-pyridineoximes [49].

The pH-dependence of the band at 400 nm may result from acidic dissociation of the HIA-Cu(II) complex, or from Cu(II) interacting solely with oximate ions. In the first case, most (if not all) of the complex would be stable at low pH, although with no spectrophotometric evidence. In the latter case, instead, one would expect complex disruption and release of free Cu(II) at a pH low enough to suppress HIA dissociation.

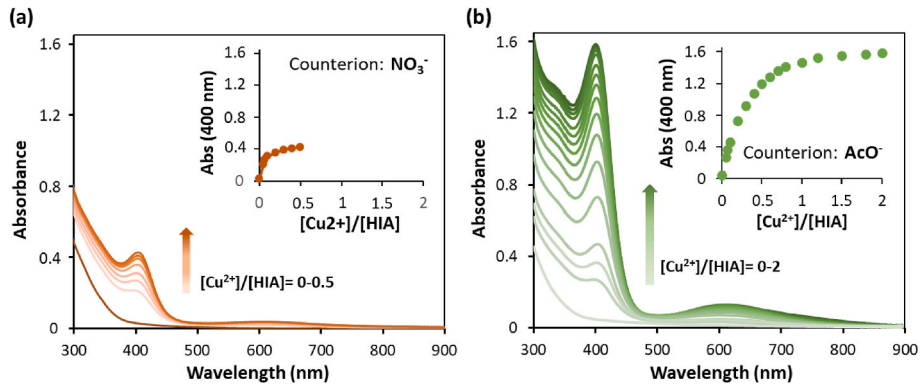


**Fig. 2.** Absorption spectra in water of (a) $Cu(NO_3)_2$/**$H_{38}$-*b*-G4$_{75}$** and (b) $Cu(OAc)_2$/**$H_{38}$-*b*-G4$_{75}$** (PIM) [HIA] = 1.8 mM solutions at increasing concentrations of Cu(II) recorded after 5 min from each addition.

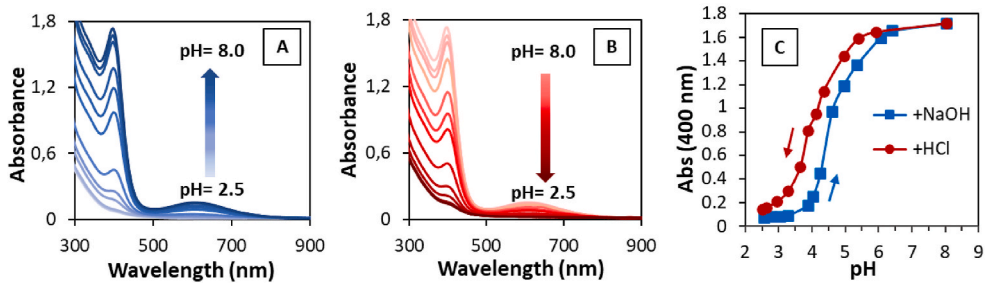


**Fig. 3.** Absorption spectra in water for $Cu(NO_3)_2$/**$H_{38}$-*b*-G4$_{75}$** ([HIA] = 1.8 mM; $[Cu^{2+}]$/[HIA] = 0.5) (A) starting from pH 2.5 and adding NaOH 0.1 M up to pH 8 and (B) subsequent addition of HCl 0.1 M. (C) Absorbance at 400 nm as a function of the pH. Measurements carried out with a cell with an optical path length of 1 cm. The spectra are corrected for dilution.

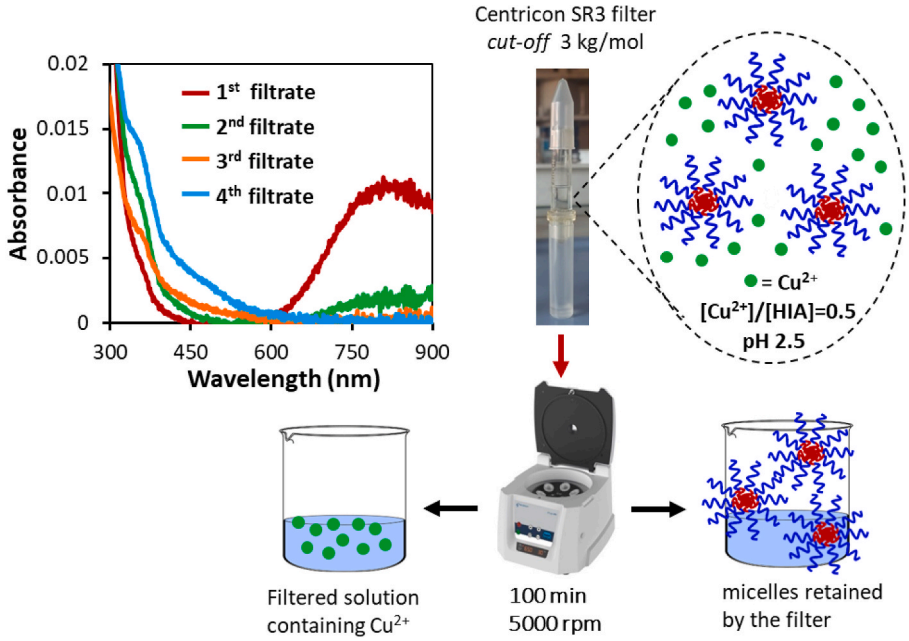


**Fig. 4.** Schematic of centrifugal filtration process for the **$H_{38}$-*b*-G4$_{75}$** complexed micelle solution ([HIA] = 1.8 mM) with $[Cu^{2+}]$/[HIA] = 0.5 at pH 2.5 with the UV–Vis spectra after the four filtrations.

With this in mind, we resorted to centrifugal filtration at acidic pH to separate the polymeric material from the bulk solution containing any Cu(II) ions released from the micelles (Fig. 4).

The sample containing Cu(II)-loaded micelles ([HIA] = 1.8 mM; Cu $(OAc)_2$ = 0.9 mM; R = 0.5) was acidified to pH 2.5 and submitted to four sequential centrifugal filtration cycles, restoring the initial volume of the micelle solution after each filtration. The absorption spectrum of the first filtrate (Fig. 4, in red) shows a band at 780 nm ($A_{780}$ = 0.01), attributed to free Cu(II) in acidic water. With $\varepsilon_{780}$ = 12 $M^{-1}$ $cm^{-1}$(Supporting Information in Ref. [50]), free Cu(II) concentration in

the filtrate is 0.8 mM, corresponding to over 90 % recovery of the Cu(II) initially added to the micelles. The band is negligible in the second filtrate and undetected in the third and fourth. The release of Cu(II) at acidic pH supports the idea that the Cu-HIA complex is unstable with undissociated HIA and that complex formation is concomitant with HIA dissociation. As for the polymeric material recovered from the centrifugal filter, DLS analysis showed that the release of Cu(II) does not disrupt the micelles. In fact, the diameter of the nanoaggregates remains constant at 30 nm throughout the complexation-release experiment, confirming that core crosslinking by Cu(II) ions (*vide infra* for Cu-loaded micelles characterization) is gradually replaced by the formation of hydrophobic interactions of the protonated PHIABMA chains. After alkalinization at pH 12.0, DLS analysis showed complete disassembly of the recovered micelles, consistently with pristine, unloaded pH-sensitive micelles [35]. On the other hand, a precipitate formed upon alkalinization of the first filtrate, thus confirming that no polymer is present to stabilize Cu(II). In short, the micellar complexes effectively release Cu (II) at acidic pH and the polymer and metal ions can be separated by simple centrifugation or dialysis. Interestingly, this would constitute a recyclable system for copper uptake and release.

Based on the results outlined so far, optimal Cu(II) loading of the micelles should be obtained at suitable pH values granting quantitative dissociation of the Cu(II)-HIA complexes. For this reason, in order to assess the stoichiometry of Cu(II)-oximate complex, increasing aliquots of $Cu(OAc)_2$ in 0.015 M phosphate buffer at pH 7, i.e. well above the pKa of 4.65, were added to $\mathbf{H_{38}}$-***b***-$\mathbf{G4_{75}}$ micelles, also diluted in phosphate buffer 0.015 M (final [HIA] = 1.6 mM). $A_{400}$ increases linearly up to R = 0.5, then a plateau of $A_{400}$ = 1.5 is attained. This value (considering the slight dilution of the micelles in the buffered experiment) is comparable to that reached at pH ≥ 7 in the variable pH experiments shown in Fig. 3 and S2 ($A_{400}$ = 1.6–1.7, respectively, with [HIA] = 1.8 mM), where R = 0.5. These results indicate nearly quantitative incorporation of Cu(II) ions into the micellar core up to R = 0.5, then free Cu(II) is expected to be present upon further additions of metal ion.

Indeed, when samples obtained from $Cu(OAc)_2$/$\mathbf{H_{38}}$-***b***-$\mathbf{G4_{75}}$ with R = 0.1–2 were submitted to centrifugal filtration 24 h after preparation, the band of free Cu(II) at 780 nm was below detection in the filtrates at R = 0.1–0.5, then it increased linearly up to R = 2 (Figs. 4 and 5b). This experiment confirms that, within detection limits with such small extinction coefficient ($\varepsilon$ = 12 $M^{-1}cm^{-1}$) [50], the metal ions are quantitatively incorporated into the micelles until a stoichiometry of two HIA groups for each Cu(II) ion is reached. At R > 0.5, 70 % of the exceeding Cu(II) is found as free ions in the filtrate, so a 30 % fraction is loaded into the micelles without increasing the intensity of the $A_{400}$ band (Fig. 5a). The limited incorporation of Cu(II) exceeding the 1:2 stoichiometry may be explained by the lesser stability of 1:1 [$Cu^{2+}$]/[HIA] complexes, whereas the constant value of $A_{400}$ is amenable to the constant concentration of quantitatively dissociated HIA groups interacting with Cu (II), regardless of complex stoichiometry.

We then studied more in detail the kinetics of complex formation at [$Cu(OAc)_2$]/[HIA] = 0.5 ratio, as shown in Fig. 6. In fact, In order for the complex to form, Cu(II) ions need to migrate through the micelle corona and into the core, where oxime acidic dissociation and metal complexation may trigger segmental reorganizations.

In only 10 s the absorbance had already reached approximatively 70 % of the end-point (0.9 *vs.* 1.3), then a slower phase followed, with about 90 % of the final absorbance reached after less than 10 min. This result confirms that most of the Cu(II) is complexed in the micelle *core* within few minutes, despite the need to reach the coordination sites.

The data were fitted according to a multi-exponential decay function of characteristic times of the type [51,52]:

$$Abs = Abs_{max} * \left(1 - a_1 \exp\left(-\frac{t}{t_1}\right) - a_2 \exp\left(-\frac{t}{t_2}\right) - a_3 \exp\left(-\frac{t}{t_3}\right)\right)$$

By interpolating the experimental curve, we obtained three characteristic times, $t_1$ = 2.2 s associated with approximately 71 % of the signal, $t_2$ = 91.5 s associated with a further 17 % increase, then the final signal is reached with $t_3$ = 71 min. The shorter time $t_1$ should correspond to the rapid diffusion of ions within the core of the micelles reaching the coordination positions without the need for significant rearrangement of the polymer chains. The longer characteristic time $t_2$, of about 1.5 min is in keeping with those generally observed in the formation of micelles from polyelectrolytes [53] and is reasonably representative of the rearrangement of some short or medium range polymeric segments necessary to make additional coordination sites available to other metal

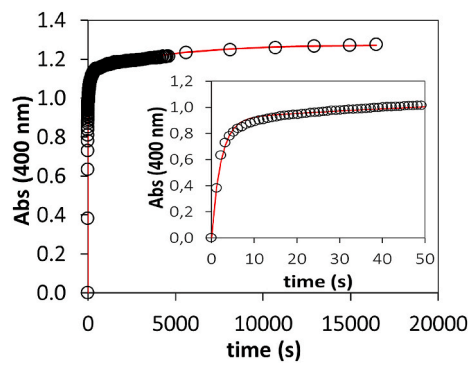


**Fig. 6.** Absorbance trend at 400 nm as a function of time during complexation of $\mathbf{H_{38}}$-***b***-$\mathbf{G4_{75}}$ micelles ([HIA] = 1.8 mM; $Cu(OAc)_2$ with [$Cu^{2+}$]/[HIA] = 0.5 ratio; empty blue circles) interpolated with multi-exponential decay function (red line). The first 50 s are shown in the inset. Measurements carried out with a cell with an optical path length of 1 cm. (For interpretation of the references to color in this figure legend, the reader is referred to the Web version of this article.)

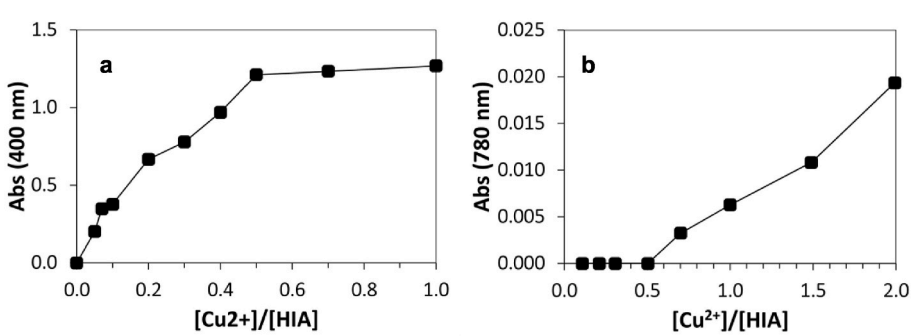


**Fig. 5.** Loading of Cu(II) by pre-formed micelles of $\mathbf{H_{38}}$-***b***-$\mathbf{G4_{75}}$. ([HIA] = 1.6 mM) in phosphate buffer 0.015 M at pH 7. (a) $A_{400}$ recorded 5 min after addition of aliquots of $Cu(OAc)_2$ (50 mM in phosphate buffer 0.015 M at pH 7) to pre-formed micelles of $\mathbf{H_{38}}$-***b***-$\mathbf{G4_{75}}$ in the same buffer. (b) $A_{780}$ (free Cu(II) band) of the filtrate obtained by centrifugal filtration of Cu(II)-loaded micelles at different [$Cu^{2+}$]/[HIA].

ions entering the micelle core. The third and longest $t_3$ is associated with the last 11 % interactions most probably taking place with even more complex rearrangements or displacements of the polymeric chains over a longer range.

### 3.2. Characterization of Cu(II)-loaded micelles

All data shown below are referred to the micellar complex obtained with $Cu(OAc)_2$.The dimensions of the complexed micelles with R = 0.5 were measured by DLS. At t = 24 h after Cu(II) addition, the $D_h$ was about 30 nm, almost identical, within the experimental error, to that of the copper-free micelles (Fig. 7). This reasonably indicates that the size of the micelles core remains essentially unchanged after complexation, with the outer POEGMA shell effectively preventing intermicellar interactions.

The STEM image obtained without staining allows to visualize selectively the PHIABMA core of the micelles thanks to the significant contrast increase provided by the complexed Cu(II) ions. The image shows the presence of dark circular particles with a diameter of about 10 nm (Fig. 7b). As expected, the diameter of the core is smaller than the overall diameter of the micelle obtained by DLS measurements (30 nm, Fig. 7a) and from TEM measurements with negative staining (24 nm, as reported in our previous work). The thickness of the POEGMA outer shell is therefore between 6 and 10 nm.

The SAXS data collected for **$H_{38}$-*b*-$G4_{75}$** micelles complexed with $[Cu^{2+}]/[HIA] = 0.2$ and 0.5 confirm the spherical shape and the same geometrical parameters as those of the unloaded micelles, with a maximum size of 29.5 ± 0.5 nm and a gyration radius $R_g$ of the order of 9 nm (Table S1). Compared to the copper-free PIM micellar system (Fig. 8, red dots), SAXS data record an increase of the scattered intensity, which can be explained by a larger overall electron density contrast of the micelles relative to the solvent, consistent with the incorporation of Cu(II) ions. In addition to the initial decay of intensity related to the overall micellar size, the high q portion of the profiles ($q > 0.5\ nm^{-1}$) follows a characteristic slope relating to the scattering of polymer chains, arising from the POEGMA shell. An analytical model for a block copolymer micelle comprising a spherical compact core (with diameter from 9 to 11 nm) grafted with chains having radius of gyration of the order of 3 nm is in agreement with the experimental data, and, keeping constant the aggregation number (equal to 46) and the concentration of micelles as in the unloaded sample, the changes observed with increasing Cu(II) concentration are consistent with increased electron density values and increased relative scattering contribution from the spherical core.

The well-defined *core-shell* structure of the Cu(II)-loaded micelles is further confirmed by their thermoresponsive behavior. In our previous work [35] we showed that micelles of **$H_{38}$-*b*-$G4_{75}$** obtained with the PIM method have well-defined *cores* and *shells* and they show a sharp transition at $T_{CP}$ = 57 °C (90 % of trasmittance at $\lambda$ = 700 nm) in their turbidimetric profile. Here, we repeated the experiment with Cu (II)-loaded micelles (R = 0.5) and found the same sharp drop of transmittance within 1 °C of the $T_{CP}$ of the pristine micelles (Fig. 9).

Moreover, DLS temperature scans were carried out on the complexed micelle solution. DLS analysis showed an increase in micelle diameters (up to 500 nm) in correspondence to the $T_{CP}$. Cooling the solution back to 25 °C, upon gentle shaking, it became clear again Fig. S4 in less than 2 min (Fig. S4). Somewhat larger nanoparticles than the starting ones were observed a few minutes after cooling to 25 °C, with $D_h$ about 55 nm, but the size decreased to 37 nm after 30 min and to 31 nm after 17 h. The SAXS data (Fig. 10) obtained at 25 °C before and after heating at 65 °C, highlighted in both cases the presence of the Cu(II)-loaded block copolymer micelles with unchanged size ($R_g$ 9 nm, $D_{max}$ 30 nm). The slightly more anisotropic shape of the pair distance distribution function detected after the heating-cooling cycle (inset in Fig. 10a) might be due to a small fraction of clustered micelles, as also suggested by the STEM images acquired without contrast agent after heating (Fig. 10b).

From these observations, it is possible to envisage a recyclable micellar thermoresponsive system for the recovery of Cu(II).

### 3.3. Formation of Cu° nanoparticles by reduction of Cu(II)

Ascorbic acid (AA) at pH 7 was used to reduce Cu(II) complexed in **$H_{38}$-*b*-$G4_{75}$** PIM micelles, R = 0.5. As can be seen in Fig. 11, the addition of AA in molar excess (6:1) leads to the loss of the green color of the solution (band at 610 nm) and to the disappearance of the band at 400 nm. TEM images (Fig. 11b) show spherical particles with a size of 5–10 nm, similar to those obtained for PIM complexed with Cu(II). Electron diffractogram of the NPs was obtained by the NED technique (Fig. S5). Micellar complexes with Cu(II) are amorphous and do not exhibit nanodiffraction, whereas after reduction with AA, typical diffractograms of polycrystalline samples, with well-defined rings and spots corresponding to the various lattice planes, are observed. Calibration with standard samples allowed us to verify the presence of a brighter and sharper ring corresponding to the lattice planes (111) of metallic copper. This result paves the way to further investigations on the stability of the obtained core-shell nanoparticles, which are increasingly investigated for biomedical applications, photonics, catalysis and templated nanoclusters [16–19].

### 3.4. Copper-induced nanoaggregation

In our previous investigation [35], we have shown that the block copolymer **$H_{38}$-*b*-$G4_{75}$** is insoluble as such in neutral water and can only be stabilized in aqueous solution as a micellar nanoaggregate. On the

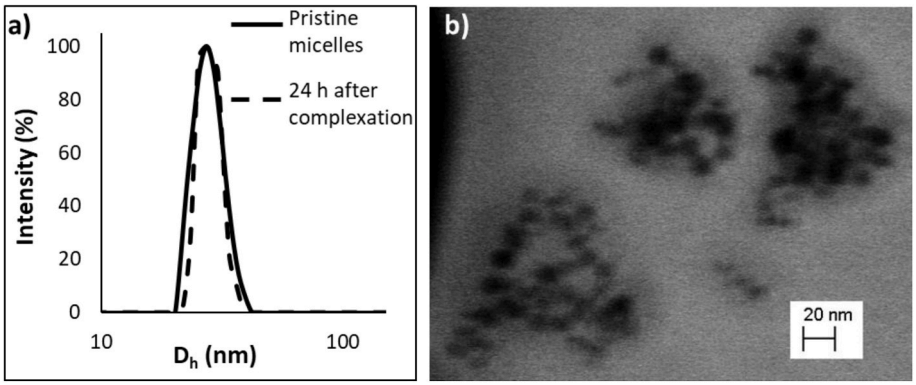


**Fig. 7.** (a) Size distribution obtained using the CONTIN method for **$H_{38}$-*b*-$G4_{75}$** uncomplexed micelles (in black) and $Cu^{2+}$/**$H_{38}$-*b*-$G4_{75}$** complexed micelles with $[Cu^{2+}]/[HIA] = 0.5$ (dashed line) (25 °C, 90°, 200 slit, filtration x1 with PTFE filters). (b) STEM image of $Cu^{2+}$/**$H_{38}$-*b*-$G4_{75}$** complexed micelles with $[Cu^{2+}]/[HIA] = 0.5$ on 0.3 mg $mL^{-1}$ without staining.

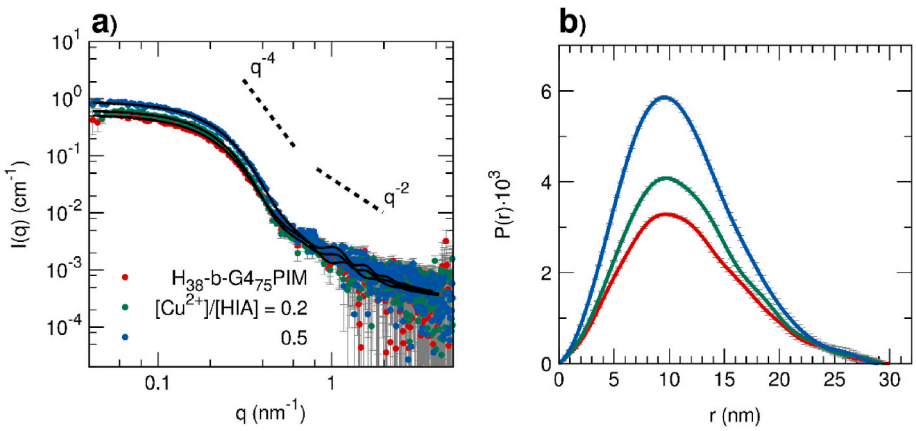


**Fig. 8.** a) SAXS data of PIM of $\mathbf{H_{38}}$-***b***-$\mathbf{G4_{75}}$ ([HIA] = 1.8 mM) (red dots), of $\mathbf{H_{38}}$-***b***-$\mathbf{G4_{75}}$/Cu(OAc)$_2$ for [$Cu^{2+}$]/[HIA] = 0.2 (green dots) and 0.5 (blue dots) and model intensity according to a block copolymer micelle form factor (parameters reported in Table S2a); b) Pair distance distribution functions P(r) obtained by means of the indirect Fourier transform of the SAXS data. (For interpretation of the references to color in this figure legend, the reader is referred to the Web version of this article.)

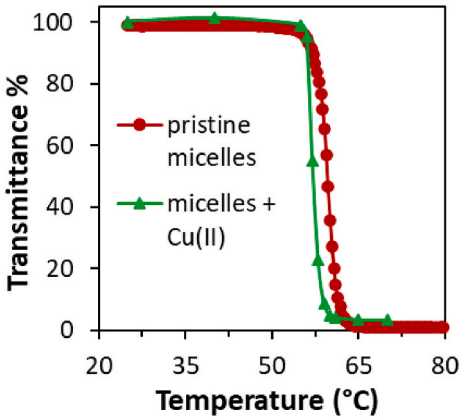


**Fig. 9.** Turbidimetric measurement on 1.5 mg mL$^{-1}$ $Cu^{2+}$/$\mathbf{H_{38}}$-***b***-$\mathbf{G4_{75}}$ micellar system in water with [$Cu^{2+}$]/[HIA] = 0.5 ratio (green line), compared to those on pristine $\mathbf{H_{38}}$-***b***-$\mathbf{G4_{75}}$ micelles (red line). $\lambda$ = 700 nm; heating rate of 1 °C min$^{-1}$. (For interpretation of the references to color in this figure legend, the reader is referred to the Web version of this article.)

other hand, it is fully soluble in many organic solvents, including acetonitrile (ACN). Based on previous work in our group showing that the HIA group is able to form complexes with Cu(II) in acetonitrile [38], we studied the Cu(II)-polymer interaction in acetonitrile with $\mathbf{H_{38}}$-***b***-$\mathbf{G4_{75}}$ and with the $\mathbf{H_{40}}$ homopolymer (Fig. 1). Specifically, we investigated whether complexation with Cu(II) would induce nano-aggregation into hybrid polymeric micelles, in view of potential applications as catalytic nanoreactors in organic solvents, with size-based recovery of the polymeric catalyst. Several aliquots of a Cu(OAc)$_2$ solution (10 mg mL$^{-1}$) were added to the polymer solutions in ACN ([HIA] = 1 mM), spanning R = 0.05 to 2. UV–Vis spectra confirmed the formation of the complex (Fig. 12), with a narrow and intense band appearing at 414 nm and a broader one at 616 nm, similarly to the ones observed in water.

With both HIA-containing polymers, the position of the band around 616 nm remains constant until R = 0.5 is reached, then it shifts towards longer wavelengths (insets in Fig. 12), due to the overlap of the 670 nm band of free Cu(OAc)$_2$ in ACN. Analogously, a shift towards shorter wavelengths is observed for the 414 nm band, due to overlap with the 375 nm absorption of free Cu(OAc)$_2$ in ACN. Plotting the absorbance of the band at 414 nm as a function of R, a linear trend is observed up to R = 0.4, then the curves flatten out beyond R = 0.5 (Fig. 12c). This is compatible with the formation of a complex in which each Cu(II) is coordinated by two HIA groups. In fact, the 1:2 metal/ligand stoichiometry is confirmed with the Job graphical method (Fig. S6). The small increase in absorbance up to R = 2 is attributed to free copper in solution (375 nm band of Cu(OAc)$_2$ in acetonitrile). From the slope of the linear part of the graphs in Fig. 12 we calculated $\boldsymbol{\varepsilon}$ = 2060 M$^{-1}$cm$^{-1}$ for $\mathbf{H_{38}}$-***b***-$\mathbf{G4_{75}}$ and $\boldsymbol{\varepsilon}$ = 1530 M$^{-1}$cm$^{-1}$ for $\mathbf{H_{40}}$. These values are very close to those obtained with pre-formed micelles in water, as discussed above. When a 4-fold excess TFA in ACN was added to the $Cu^{2+}$/$\mathbf{H_{38}}$-***b***-$\mathbf{G4_{75}}$ complex (R = 2), the intensities of the bands of the complex decreased

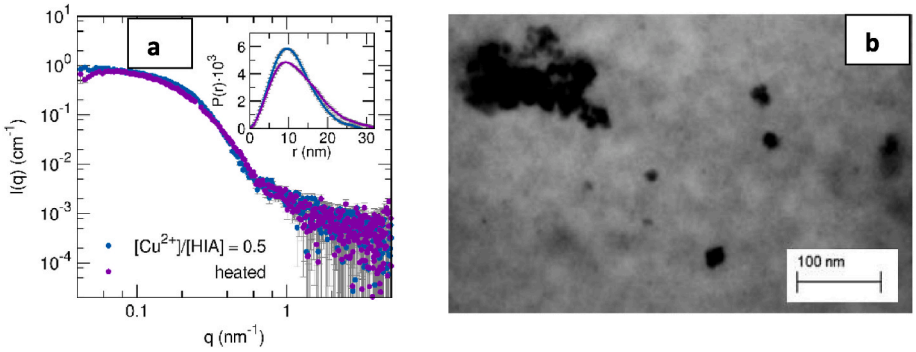


**Fig. 10.** a) The SAXS data of $\mathbf{H_{38}}$-***b***-$\mathbf{G4_{75}}$/Cu(OAc)$_2$ ([HIA] = 1.8 mM) with [$Cu^{2+}$]/[HIA] = 0.5 collected at 25 °C before (blue dots) and after (purple dots) a heating cycle up to 65 °C. In the inset, the corresponding pair distance distribution functions are reported; b) STEM images without contrast agent of Cu(OAc)$_2$/$\mathbf{H_{38}}$-***b***-$\mathbf{G4_{75}}$ PIM micelles ([HIA] = 1.8 mM; [$Cu^{2+}$]/[HIA] = 0.5) taken at 25 °C after heating to 65 °C. (For interpretation of the references to color in this figure legend, the reader is referred to the Web version of this article.)

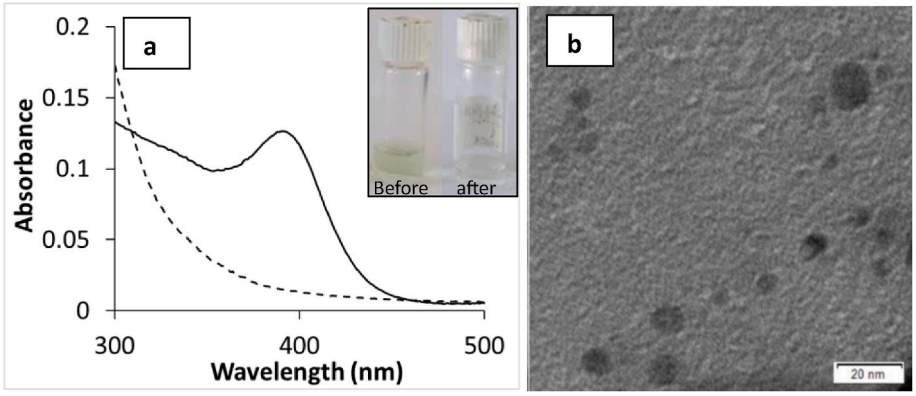


**Fig. 11.** a) Absorption spectra of **$H_{38}$-*b*-G4$_{75}$** PIM micelles complexes with Cu(II), [$Cu^{2+}$]/[HIA] = 0.5, ([HIA = 1.8 mM) before (full line) and after (dashed line) reduction with L-ascorbic acid ([AA]/[$Cu^{2+}$] = 6, t = 5 days) at pH = 7. Measurements made with a cell with an optical path of 0.1 cm. b) TEM image of the Cu° nanoparticles without contrast agent.

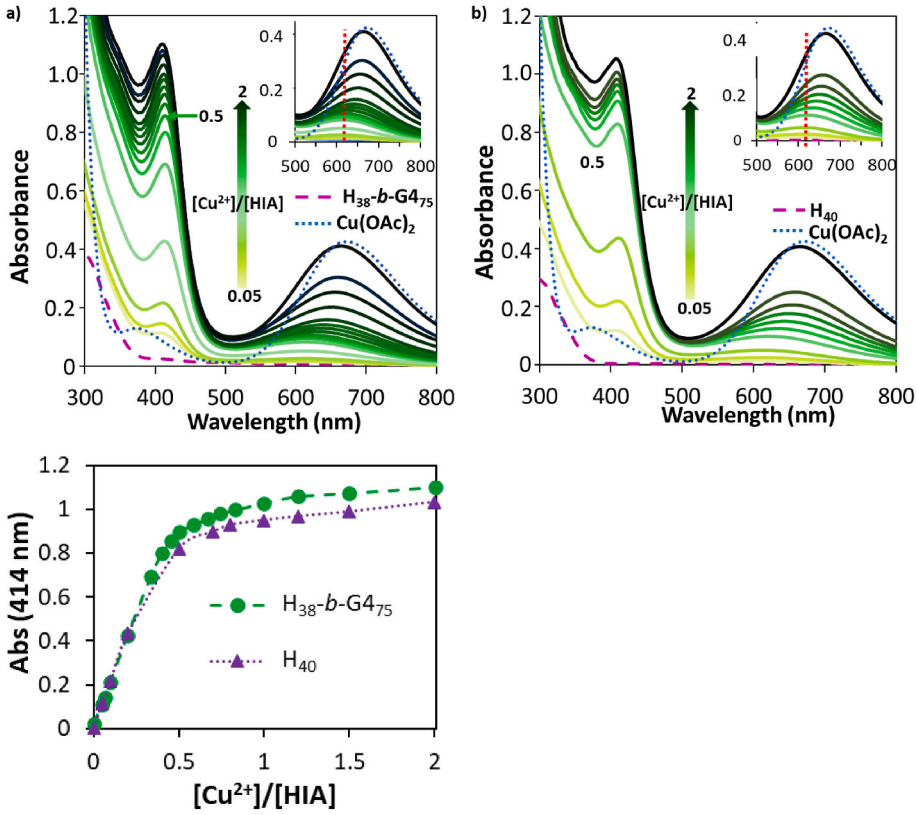


**Fig. 12.** (a) Absorption spectra in acetonitrile of: $Cu(OAc)_2$ (1.9 mM, blue dotted line), **$H_{38}$-*b*-G4$_{75}$** ([HIA] = 1 mM, violet dashed line); $Cu(OAc)_2$/**$H_{38}$-*b*-G4$_{75}$** as the ratio [$Cu^{2+}$]/[HIA] increases from 0.05 to 2. Cuvette with optical path length 1 cm. (b) Absorption spectra in acetonitrile of: $Cu(OAc)_2$ (1.9 mM, in blue), $H_{40}$ ([HIA] = 1 mM, in violet); $Cu(OAc)_2$/$H_{40}$ as the ratio [$Cu^{2+}$]/[HIA] increases from 0.05 to 2. Cuvette with optical path length 1 cm. (c) Absorbance trend of the 414 nm band in ACN as a function of the [$Cu^{2+}$]/[HIA] molar ratio for a) $Cu(OAc)_2$/**$H_{38}$-*b*-G4$_{75}$** and b) $Cu(OAc)_2$/$H_{40}$. (For interpretation of the references to color in this figure legend, the reader is referred to the Web version of this article.)

significantly. Furthermore, the maximum of the *d-d* band shifted at longer wavelengths, as expected in the presence of free Cu(II)-TFA complexes [54] (Fig. S7). Interestingly, when **MH$_{25}$-*b*-G4$_{75}$** (Fig. 1) is used in place of **$H_{38}$-*b*-G4$_{75}$**, the characteristic bands of the complex at 414 and 616 nm fail to appear and the spectrum is fully consistent with that of free $Cu(OAc)_2$ in ACN (Fig. S8). In fact, **MH$_{25}$-*b*-G4$_{75}$**, which is the O-methylated analogue of **$H_{38}$-*b*-G4$_{75}$**, cannot dissociate into oximate anions. These results confirm the role of the oximate ion in complex formation in ACN as well as in water.

DLS analysis shows that Cu(II) complexation induces nanoaggregation of both **$H_{38}$-*b*-G4$_{75}$** and **$H_{40}$** polymers in ACN. At R = 0.5, nanoaggregates of $D_h$ = 20 nm ca. are detected with both polymers (Fig. 13a and b). The presence of a larger albeit quantitatively negligible population is observed before filtration of the samples. The TEM images obtained with Cu(II)–**$H_{38}$-*b*-G4$_{75}$** using phosphotungstic acid (PTA) as negative stain for the entire nanoaggregates allow the observation of spherical objects of about 18 nm (Fig. 13c). Without staining, where dark contrast is provided by Cu(II) only, the observed spherical objects (Fig. 13d) exhibit a smaller diameter of 10–12 nm. This result is in keeping with a core-shell structure of the aggregates induced by Cu(II)

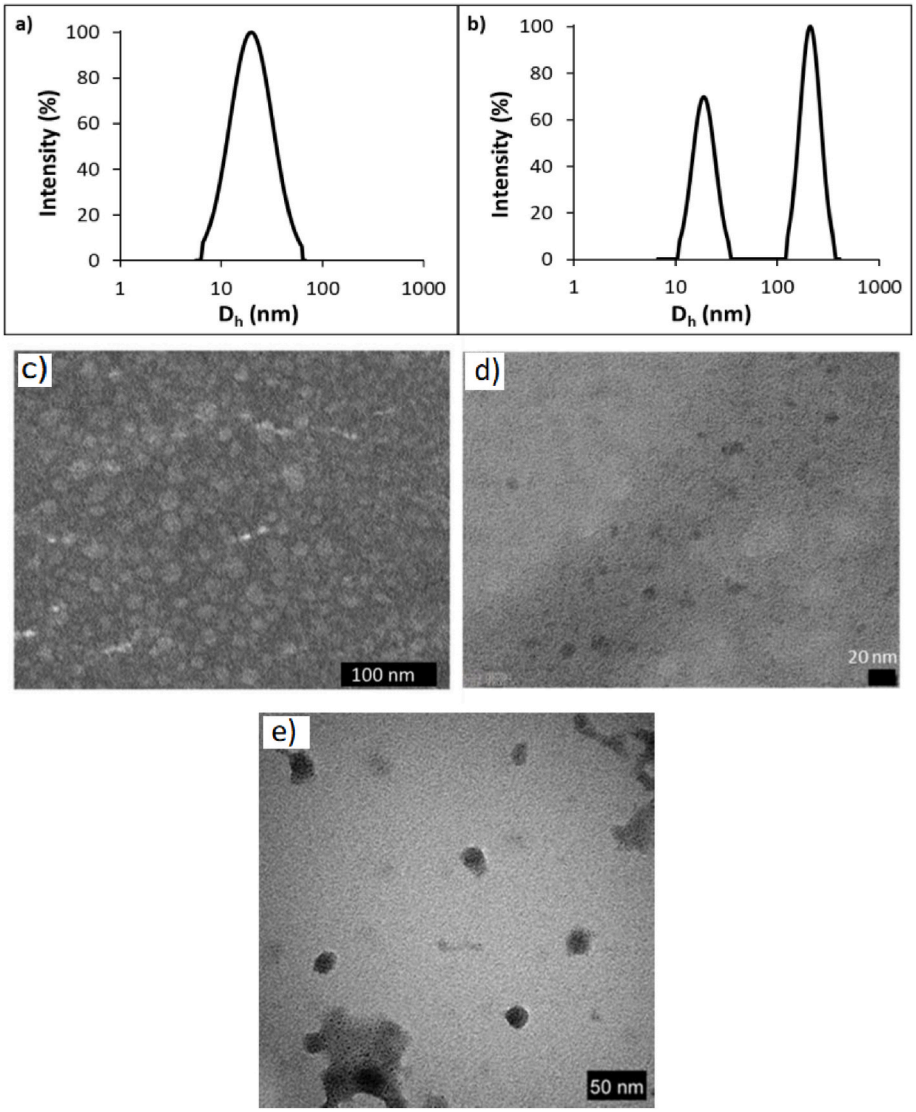


**Fig. 13.** Size distribution obtained using the CONTIN method for a) $Cu^{2+}$/**$H_{38}$-*b*-G4$_{75}$** complex (25 °C, 90°, 400 slit, filtration x1 with PTFE filters) and b) $Cu^{2+}$/**$H_{40}$** complex (25 °C, 90°, slit 200, without filtration). TEM image of $Cu^{2+}$/**$H_{38}$-*b*-G4$_{75}$** complex in acetonitrile ([HIA] = 1 mM; [$Cu^{2+}$]/[HIA] = 0.5): c) image acquired with PTA as contrast agent and d) without contrast agent. e) TEM image of the $Cu^{2+}$/**$H_{40}$** complex in acetonitrile with [HIA] = 4 mM and [$Cu^{2+}$]/[HIA] = 0.5 acquired without contrast agent.

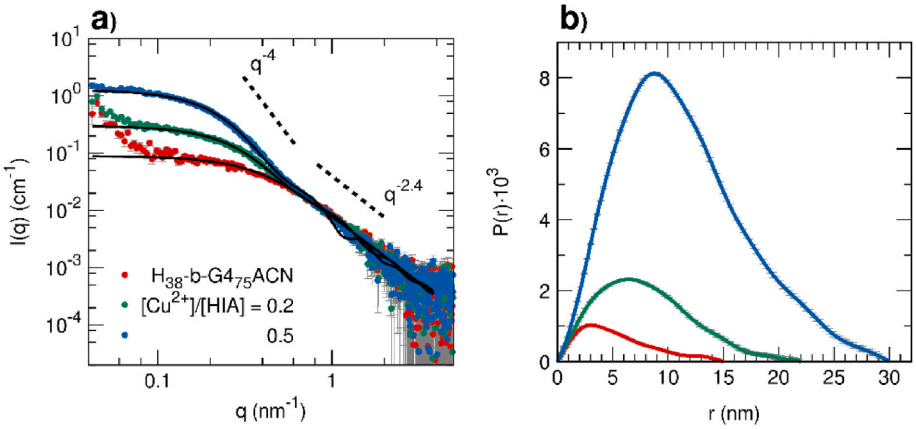


**Fig. 14.** a) SAXS data of **$H_{38}$-*b*-G4$_{75}$** ([HIA] = 1.8 mM) in ACN (red dots), of **$H_{38}$-*b*-G4$_{75}$**/$Cu(OAc)_2$ in the same solvent for [$Cu^{2+}$]/[HIA] = 0.2 (green dots) and 0.5 (blue dots) and model intensity according to a chain form factor (without Cu(II)) and a block copolymer micelle form factor (parameters reported in Table S2b); b) Pair distance distribution functions P(r) obtained by means of the indirect Fourier transform of the SAXS data. (For interpretation of the references to color in this figure legend, the reader is referred to the Web version of this article.)

complexation in ACN. In fact, since Cu(II) does not bind to POEGMA, visualization of the micelle core is provided by the Cu(II) ions in the absence of staining. Regarding Cu(II)–$\mathbf{H_{40}}$, we find it quite surprising that small aggregates would form in ACN, i.e. in the absence of stabilizing POEGMA blocks. However, this result is confirmed by TEM in the absence of staining, as shown in Fig. 13e.

SAXS was also used to characterize $\mathbf{H_{38}}$-***b***-$\mathbf{G4_{75}}$ ([HIA] = 1.8 mM) in ACN solution before and after complexation with $Cu(OAc)_2$ (Fig. 14). For the free polymer the data are in agreement with individual chains having $R_g$ of 4 nm and a characteristic intensity decay at large q with Flory exponent of 0.42 ($I(q) \propto q^{-1/0.42}$) suggesting conditions only slightly less swollen compared to the theta solvent ($I(q) \propto q^{-1/0.5}$). Upon addition of $Cu(OAc)_2$, the low q intensity progressively grows, indicating the formation of aggregates with average $R_g$ of 6 and 9 nm and maximum sizes of 20 and 30 nm for R = 0.2 and 0.5, respectively. On the other hand, the scattering signal for $q > 0.5\ nm^{-1}$ remains almost superimposable to that observed for the free chains in absence of Cu(II), suggesting that the copolymer preserves its flexible nature and contributes similarly to the overall scattering both if free and if involved in the Cu(II)-induced aggregates. The scattering profiles can be described with similar agreement both considering only the presence of small block-copolymer micelles (with aggregation numbers of 7 and 23 for R = 0.2 and 0.5, respectively, Fig. 14a) or assuming the coexistence of free chains (in decreasing amount when increasing Cu(II) concentration) and larger micelles (aggregation numbers 23 and 28). This second assumption (Fig. S11) would be more in agreement with the overall known concentration in the sample and the aggregates observed in micrographs. However it is possible that the dropwise addition of $Cu(OAc)_2$ gives rise to a complex distribution of aggregation numbers.

## 4. Conclusions

We have demonstrated the formation, both in water and in acetonitrile, of hybrid Cu(II)-polymer nanoaggregates through complexation by oximate groups in 4-[hydroxyimino)aldehyde]butyl methacrylate polymers and copolymers. Cu(II)-loaded micelles can be obtained either by fast migration of metal ions into pre-formed micelles, or by spontaneous nanoaggregation of free polymer chains induced by Cu(II) complexation. DLS, TEM and SAXS analyses show spherical *core-shell* structures of 18–30 nm overall diameter with Cu(II) located in 5–10 nm micelle core, specific sizes being dependent of the preparation method. In water, the acidity of the ligand groups is dramatically enhanced (about 6.5 orders of magnitude) by the interaction with Cu(II), in keeping with similar results described in the literature for other oximes. Complex formation involves oximate ions with a 1:2 Cu(II)/ligand optimal stoichiometry. The hybrid micelles retain the thermoresponsivity of the PTEGMA shell, thus providing a means for their physical separation at about 55 °C. Regarding metal release, Cu(II) is freed from the polymeric micelles in acidic conditions and can be selectively recovered by centrifugal filtration. In fact, unlike other polyelectrolyte systems that disassemble upon metal release, the polymeric micelles described herein are unaltered by the uptake/release process. A recyclable system for metal uptake and recovery is thereby envisaged. Furthermore, we have obtained $Cu^0$ nanoparticles in water through reduction with ascorbic acid of the Cu(II) ions in the polymeric complex. This result is relevant in view of the many currently investigated applications of $Cu^0$ nanoparticles, such as biomedical, photonics, catalysis, and templated nanoclusters.

## Funding

This research was partially funded by the NRRP Next Generation EU project (Project code PE00000007) "One Health Basic and Translation Research Actions addressing unmet Needs on Emerging Infectious Diseases, INF-ACT"; Sapienza University of Rome (research grant number B89C20002540001 and RM1221816C7F5D4C); the Italian National Research Council (CNR) (NUTRAGE grant number FOE-2021 DBA. AD005.225).

A.D.G. acknowledges co-financing of Sapienza University of Rome and the European Union—FSE-REACT-EU, PON Research and Innovation 2014–2020 DM1062/2021 for the RTD-A contract 26-G-15245-1.

## CRediT authorship contribution statement

**Irene Antignano:** Writing – original draft, Methodology, Investigation, Formal analysis, Data curation, Conceptualization. **Stefano Casciardi:** Investigation. **Francesca D'Acunzo:** Writing – review & editing, Supervision, Methodology, Investigation, Funding acquisition, Formal analysis, Data curation, Conceptualization. **Alessandra Del Giudice:** Visualization, Methodology, Investigation, Formal analysis. **Laura Gatti:** Investigation. **Patrizia Gentili:** Supervision, Methodology, Funding acquisition, Conceptualization. **Francesco Mura:** Visualization, Investigation, Formal analysis. **Agnese Ricci:** Investigation. **Giancarlo Masci:** Writing – review & editing, Supervision, Methodology, Investigation, Funding acquisition, Formal analysis, Data curation, Conceptualization.

## Declaration of competing interest

The authors declare that they have no known competing financial interests or personal relationships that could have appeared to influence the work reported in this paper.

## Data availability

Data will be made available on request.

## Acknowledgements

The Sapienza Research Infrastructure is acknowledged for the SAXS measurements at SAXSLab Sapienza, funded by the Large Equipment Project 2015-C26J15BX54. The authors would like to thank Prof. Antonio D'Alessandro, Director of the Centre of Nanotechnologies Applied to Engineering–CNIS, Sapienza University of Rome for access to the electron microscopy facility.

## Appendix A. Supplementary data

Supplementary data to this article can be found online at https://doi.org/10.1016/j.polymer.2024.127197.

## References

[1] F. D'Acunzo, G. Masci, Playing construction with the monomer toy box for the synthesis of multi-stimuli responsive copolymers by reversible deactivation radical polymerization protocols, J. Polym. Sci. 59 (24) (2021) 3059–3083, https://doi.org/10.1002/POL.20210590.

[2] P. Schattling, F.D. Jochum, P. Theato, Multi-stimuli responsive polymers – the all-in-one talents, Polym. Chem. 5 (1) (2013) 25–36, https://doi.org/10.1039/C3PY00880K.

[3] S.S. Das, P. Bharadwaj, M. Bilal, M. Barani, A. Rahdar, P. Taboada, S. Bungau, G. Z. Kyzas, Stimuli-responsive polymeric nanocarriers for drug delivery, imaging, and theragnosis, Polymers 12 (6) (2020) 1397, https://doi.org/10.3390/polym12061397.

[4] A. Nabiyan, J.B. Max, F.H. Schacher, Double hydrophilic copolymers-synthetic approaches, architectural variety, and current application fields, Chem. Soc. Rev. 51 (3) (2022) 995–1044, https://doi.org/10.1039/d1cs00086a.

[5] Y. Dai, P. Wu, Exploring the influence of the poly(4-vinyl pyridine) segment on the solution properties and thermal phase behaviours of oligo(ethylene glycol) methacrylate-based block copolymers: the different aggregation processes with various morphologies, Phys. Chem. Chem. Phys. 18 (31) (2016) 21360–21370, https://doi.org/10.1039/c6cp04286d.

[6] H. Mardani, H. Roghani-Mamaqani, S. Shahi, M. Salami-Kalajahi, Stimuli-responsive block copolymers as PH chemosensors by fluorescence emission intensification mechanism, Eur. Polym. J. 162 (2022) 110928, https://doi.org/10.1016/j.eurpolymj.2021.110928.

[7] H. Tabasi, M. Babaei, K. Abnous, S.M. Taghdisi, A. Sh Saljooghi, M. Ramezani, M. Alibolandi, Metal–polymer-coordinated complexes as potential nanovehicles for

drug delivery, J Nanostructure Chem 11 (4) (2021) 501–526, https://doi.org/10.1007/s40097-021-00432-7.
[8] S. Thanneeru, S.S. Duay, L. Jin, Y. Fu, A.M. Angeles-Boza, J. He, Single chain polymeric nanoparticles to promote selective hydroxylation reactions of phenol catalyzed by copper, ACS Macro Lett. 6 (7) (2017) 652–656, https://doi.org/10.1021/acsmacrolett.7b00300.
[9] M. Kanduč, W.K. Kim, R. Roa, J. Dzubiella, Modeling of stimuli-responsive nanoreactors: rational rate control towards the design of colloidal enzymes, Mol Syst Des Eng 5 (3) (2020) 602–619, https://doi.org/10.1039/c9me00106a.
[10] S. Gineste, C. Mingotaud, Double-hydrophilic block copolymer–metal ion associations: structures, properties and applications, Adv. Colloid Interface Sci. 311 (2023) 102808, https://doi.org/10.1016/j.cis.2022.102808.
[11] L. Volkmann, M. Köhler, F.H. Sobotta, M.T. Enke, J.C. Brendel, F.H. Schacher, Poly (2-Acrylamidoglycolic acid) (PAGA): controlled polymerization using RAFT and chelation of metal cations, Macromolecules 51 (18) (2018) 7284–7294, https://doi.org/10.1021/acs.macromol.8b01260.
[12] Z. Abousalman-Rezvani, H. Roghani-Mamaqani, H. Riazi, O. Abousalman-Rezvani, Water treatment using stimuli-responsive polymers, Polym. Chem. 13 (42) (2022) 5940–5964, https://doi.org/10.1039/D2PY00992G.
[13] M.L. Rahman, C.J. Fui, T.X. Ting, M.S. Sarjadi, S.E. Arshad, B. Musta, Polymer ligands derived from jute fiber for heavy metal removal from electroplating wastewater, Polymers 12 (11) (2020) 2521, https://doi.org/10.3390/polym12112521.
[14] M. Kafetzi, K.B.L. Borchert, C. Steinbach, D. Schwarz, S. Pispas, S. Schwarz, Thermoresponsive PNIPAM-b-PAA block copolymers as "smart" adsorbents of Cu (II) for water restore treatments, Colloids Surf. A Physicochem. Eng. Asp. 614 (2021) 126049, https://doi.org/10.1016/J.COLSURFA.2020.126049.
[15] M. Uchman, K. Procházka, K. Gatsouli, S. Pispas, M. Špírková, CdS-containing nano-assemblies of double hydrophilic block copolymers in water, Colloid Polym. Sci. 289 (9) (2011) 1045–1053, https://doi.org/10.1007/s00396-011-2433-9.
[16] M.B. Gawande, A. Goswami, F.-X. Felpin, T. Asefa, X. Huang, R. Silva, X. Zou, R. Zboril, R.S. Varma, Cu and Cu-based nanoparticles: synthesis and applications in catalysis, Chem. Rev. 116 (6) (2016) 3722–3811, https://doi.org/10.1021/acs.chemrev.5b00482.
[17] G. Wang, T. Liu, J. Chao, H. Jin, J. Liu, H. Zhang, W. Lyu, P. Yin, A. Al-Ghamdi, S. Wageh, B. Fu, H. Zhang, Recent advances and challenges in ultrafast photonics enabled by metal nanomaterials, Adv. Opt. Mater. 10 (11) (2022) 112898, https://doi.org/10.1002/adom.202200443.
[18] A.Q. Figueiredo, C.F. Rodrigues, N. Fernandes, D. de Melo-Diogo, I.J. Correia, A. F. Moreira, Metal-polymer nanoconjugates application in cancer imaging and therapy, Nanomaterials 12 (18) (2022) 3166, https://doi.org/10.3390/nano12183166.
[19] Z. Qiao, J. Zhang, X. Hai, Y. Yan, W. Song, S. Bi, Recent advances in templated synthesis of metal nanoclusters and their applications in biosensing, bioimaging and theranostics, Biosens. Bioelectron. 176 (2021) 112898, https://doi.org/10.1016/j.bios.2020.112898.
[20] A.S. Knight, J. Larsson, J.M. Ren, R.B. Zerdan, S. Seguin, R. Vrahas, J. Liu, G. Ren, C.J. Hawker 140, 1409−1414 downloaded via UNIVERSITA DI ROMA LA SAPIENZA on february 6, J. Am. Chem. Soc. 140 (2018) 10, https://doi.org/10.1021/jacs.7b11005.
[21] J.M. Bak, H. Lee, Use of core-cross-linked polymeric micelles induced by the selective detection of Cu(II) ions for the sustained release of a model drug, ACS Appl. Mater. Interfaces 11 (15) (2019) 14368–14375, https://doi.org/10.1021/acsami.9b02432.
[22] V.N. Kislenko, L.P. Oliynyk, Complex Formation of polyethyleneimine with copper (II), nickel(II), and cobalt(II) ions, J. Polym. Sci. Polym. Chem. 40 (7) (2002) 914–922, https://doi.org/10.1002/pola.10157.
[23] M. Kurtoğlu, E. İspir, N. Kurtoğlu, S. Toroğlu, S. Serin, New soluble coordination chain polymers of nickel(II) and copper(II) ions and their biological activity, Transit. Met. Chem. 30 (6) (2005) 765–770, https://doi.org/10.1007/s11243-005-6273-7.
[24] Y. Dai, X. Zhang, R. Zhuo, Polymeric micelles stabilized by polyethylenimine–copper ($C_2H_5N$–Cu) coordination for sustained drug release, RSC Adv. 6 (27) (2016) 22964–22968, https://doi.org/10.1039/C6RA02300B.
[25] D.S. Bolotin, N.A. Bokach, V. Yu Kukushkin, Coordination chemistry and metal-involving reactions of amidoximes: relevance to the chemistry of oximes and oxime ligands, Coord. Chem. Rev. 313 (2016) 62–93, https://doi.org/10.1016/j.ccr.2015.10.005.
[26] V.Y. Kukushkin, A.J.L. Pombeiro, Oxime and oximate metal complexes: unconventional synthesis and reactivity, Coord. Chem. Rev. 181 (1) (1999) 147–175, https://doi.org/10.1016/S0010-8545(98)00215-X.
[27] L. Croitor, E.B. Coropceanu, A.E. Masunov, H.J. Rivera-Jacquez, A.V. Siminel, V. I. Zelentsov, T. Ya Datsko, M.S. Fonari, Polymeric luminescent Zn(II) and Cd(II) dicarboxylates decorated by oxime ligands: tuning the dimensionality and adsorption capacity, Cryst. Growth Des. 14 (8) (2014) 3935–3948, https://doi.org/10.1021/cg5005402.
[28] L. Croitor, E.B. Coropceanu, M.S. Fonari, Anion–Pyridine-n-Oxime interplay to control metal–metal separations in a series of Cu(II) coordination polymers, CrystEngComm 24 (35) (2022) 6146–6154, https://doi.org/10.1039/D2CE01000C.
[29] I. Mylonas-Margaritis, A. Gérard, K. Skordi, J. Mayans, A. Tasiopoulos, P. McArdle, C. Papatriantafyllopoulou, From 1D coordination polymers to metal organic frameworks by the use of 2-pyridyl oximes, Materials 13 (18) (2020) 4084, https://doi.org/10.3390/ma13184084.
[30] N. Gerasimchuk, Chemistry and applications of cyanoximes and their metal complexes, Dalton Trans. 48 (23) (2019) 7985–8013, https://doi.org/10.1039/C9DT01057B.
[31] D. Zhao, Z. Wang, S. Lu, X. Shi, An amidoxime-functionalized polypropylene fiber: competitive removal of Cu(II), Pb(II) and Zn(II) from wastewater and subsequent sequestration in cement mortar, J. Clean. Prod. 274 (2020) 123049, https://doi.org/10.1016/j.jclepro.2020.123049.
[32] K. Saeed, S. Haider, T.J. Oh, S.Y. Park, Preparation of amidoxime-modified polyacrylonitrile (PAN-Oxime) nanofibers and their applications to metal ions adsorption, J. Membr. Sci. 322 (2) (2008) 400–405, https://doi.org/10.1016/J.MEMSCI.2008.05.062.
[33] L.D. Prabhakar, C. Umarani, Synthesis, characterization, and applications of poly (salicylaldehyde-acrylate-divinylbenzene) oxime as a chelate polymer to Ni(II), Co (II), and Cu(II) ions, J. Macromol. Sci., Pure Appl. Chem. 32 (1) (1995) 129–142, https://doi.org/10.1080/10601329508011069.
[34] T. Kojima, T. Sowa, S. Kodama, M. Sato, Y. Shigetomi, Y. Yamamoto, Adsorption behaviour and separation of copper(II) ions on cellulose triacetate polymer containing α-hydroxy oxime compounds, Anal. Chim. Acta 264 (1) (1992) 59–64, https://doi.org/10.1016/0003-2670(92)85296-I.
[35] I. Antignano, F. D'Acunzo, D. Arena, S. Casciardi, A. Del Giudice, F. Gentile, M. Pelosi, G. Masci, P. Gentili, Influence of nanoaggregation routes on the structure and thermal behavior of multiple-stimuli-responsive micelles from block copolymers of oligo(ethylene glycol) methacrylate and the weak acid [2-(Hydroxyimino)Aldehyde]Butyl methacrylate, Langmuir 38 (46) (2022) 14371–14386, https://doi.org/10.1021/acs.langmuir.2c02515.
[36] P. Gentili, M. Nardi, I. Antignano, P. Cambise, M. D'Abramo, F. D'Acunzo, A. Pinna, E. Ussia, 2-(Hydroxyimino)Aldehydes: photo- and physicochemical properties of a versatile functional group for monomer design, Chem. Eur J. 24 (30) (2018) 7683–7694, https://doi.org/10.1002/CHEM.201800059.
[37] A. Di Sabato, F. D'Acunzo, D. Filippini, F. Vetica, A. Brasiello, D. Corinti, E. Bodo, C. Michenzi, E. Panzetta, P. Gentili, Unusually chemoselective photocyclization of 2-(Hydroxyimino)Aldehydes to cyclobutanol oximes: synthetic, stereochemical, and mechanistic aspects, J. Org. Chem. 87 (21) (2022) 13803–13818, https://doi.org/10.1021/acs.joc.2c01503.
[38] F. D'Acunzo, L. Carbonaro, A.D. Cort, A. Di Sabato, D. Filippini, F. Leonelli, L. Mancini, P. Gentili, Click-connected 2-(Hydroxyimino)Aldehydes for the design of UV-responsive functional molecules, Eur. J. Org Chem. 2021 (2) (2021) 289–294, https://doi.org/10.1002/ejoc.202001303.
[39] M. Sztucki, T. Narayanan, Development of an ultra-small-angle X-ray scattering instrument for probing the microstructure and the dynamics of soft matter, J. Appl. Crystallogr. 40 (s1) (2006) s459–s462, https://doi.org/10.1107/S0021889806045833.
[40] K. Manalastas-Cantos, P.V. Konarev, N.R. Hajizadeh, A.G. Kikhney, M. V. Petoukhov, D.S. Molodenskiy, A. Panjkovich, H.D.T. Mertens, A. Gruzinov, C. Borges, D.I. Sverguna, D. Frankea, Atsas 3.0: expanded functionality and new tools for small-angle scattering data analysis, J. Appl. Crystallogr. 54 (2021) 343–355, https://doi.org/10.1107/S1600576720013412.
[41] I. Breßler, J. Kohlbrecher, A.F. Thünemann, SASfit: a tool for small-angle scattering data analysis using a library of analytical expressions, J. Appl. Crystallogr. 48 (2015) 1587–1598, https://doi.org/10.1107/S1600576715016544.
[42] A.Z. El-Sonbati, A.S. Al-Shihri, A.A. El-Bindary, Polymer complexes. XLIII. EPR, spectra, and stereochemical versatility of novel copper(II)polymer complexes, J. Inorg. Organomet. Polym. 13 (2) (2003) 99–108, https://doi.org/10.1023/A:1024176714809, 13:2 2003.
[43] B.J. Hathaway, D.E. Billing, The electronic properties and stereochemistry of mono-nuclear complexes of the copper(II) ion, Coord. Chem. Rev. 5 (2) (1970) 143–207, https://doi.org/10.1016/S0010-8545(00)80135-6.
[44] P. Comba, A. Fath, T.W. Hambley, A. Vielfort, Two different types of folding of isomeric macrocycles induced by metal ion Co-ordination, J. Chem. Soc., Dalton Trans. (10) (1997) 1691–1696, https://doi.org/10.1039/a607420k.
[45] H.B. Gray, Chemical Bonds: an Introduction to Atomic and Molecular Structure, University Science Books, 2023, https://doi.org/10.7907/rt7h-8t44.
[46] L. Sacconi, M.45. Ciampolini, Pseudo-tetrahedral structure of some α-branched copper(II) chelates with schiff bases, J. Chem. Soc. 0 (0) (1964) 276–280, https://doi.org/10.1039/JR9640000276.
[47] D. Premužić, M. Korabik, M. Hołyńska, Structure and magnetic properties of a new binuclear copper(II) complex of a tripodal oxime, J. Mol. Struct. 1059 (1) (2014) 265–270, https://doi.org/10.1016/j.molstruc.2013.12.001.
[48] D.F. Back, G.M. de Oliveira, L.A. Fontana, B.F. Ramão, D. Roman, B.A. Iglesias, One-pot synthesis, structural characterization, UV–vis and electrochemical analyses of new schiff base complexes of Fe(III), Ni(II) and Cu(II), J. Mol. Struct. 1100 (2015) 264–271, https://doi.org/10.1016/j.molstruc.2015.07.050.
[49] F. Mancin, P. Tecilla, U. Tonellato, Activation of oximic nucleophiles by coordination of transition metal ions, Eur. J. Org Chem. 2000 (6) (2000) 1045–1050, https://doi.org/10.1002/(SICI)1099-0690(200003)2000:6<1045::AID-EJOC1045>3.0.CO;2-M.
[50] A. Santoro, N. Ewa Wezynfeld, M. Vašák, W. Bal, P. Faller, Cysteine and glutathione trigger the Cu-Zn swap between Cu(Ii)-Amyloid-B4-16</Inf> peptide and Zn7</inf>-metallothionein-3, Chem. Commun. 53 (85) (2017) 11634–11637, https://doi.org/10.1039/c7cc06802f.
[51] F. Kuehn, K. Fischer, M. Schmidt, Kinetics of complex formation between DNA and cationically charged cylindrical brush polymers observed by stopped flow light scattering, Macromol. Rapid Commun. 30 (17) (2009) 1470–1476, https://doi.org/10.1002/marc.200900166.
[52] S. Gineste, B. Lonetti, M. Yon, J. Giermanska, E. Di Cola, M. Sztucki, Y. Coppel, A.-F. Mingotaud, J.-P. Chapel, J.-D. Marty, C. Mingotaud, Hybrid polymeric micelles

stabilized by gallium ions: structural investigation, J. Colloid Interface Sci. 609 (2022) 698–706, https://doi.org/10.1016/j.jcis.2021.11.077.

[53] D.V. Krogstad, N.A. Lynd, D. Miyajima, J. Gopez, C.J. Hawker, E.J. Kramer, M. V. Tirrell, Structural evolution of polyelectrolyte complex core micelles and ordered-phase bulk materials, Macromolecules 47 (22) (2014) 8026–8032, https://doi.org/10.1021/ma5017852.

[54] E.M. Glebov, V.F. Plyusnin, V.P. Grivin, S.A. Krupoder, T.I. Liskovskaya, V. S. Danilovich, Photochemistry of copper(II) polyfluorocarboxylates and copper(II) acetate as their hydrocarbon analogues, J. Photochem. Photobiol. Chem. 133 (3) (2000) 177–183, https://doi.org/10.1016/S1010-6030(00)00234-3.